

Effects of Deposition Temperature on Phase Transition of Amorphous Ice

Kentaro Kina, Yui Ono, Daiki Yoshida, and Tomoko Ikeda-Fukazawa*

Cite This: *J. Phys. Chem. C* 2024, 128, 7806–7812

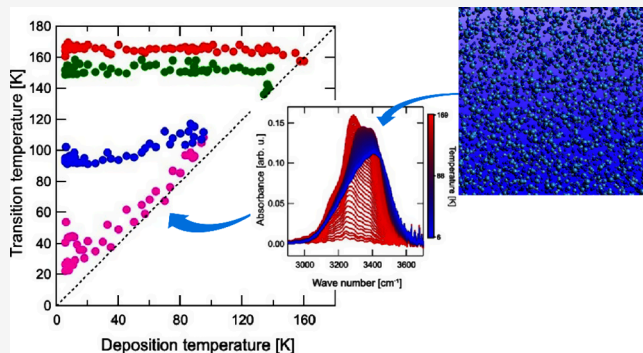
Read Online

ACCESS |

Metrics & More

Article Recommendations

ABSTRACT: To investigate the effects of deposition temperature, T_d , on the phase transition of amorphous ice with heating, the infrared spectra of ice deposited at temperatures of 6–160 K were measured. From the changing rate of the wavenumber of the O–H symmetric stretching mode with heating, the transition processes from high-density amorphous (HDA) ice to crystalline hexagonal ice I_h via low-density amorphous (LDA) ice and ice I_c were analyzed. The results show that the structure of the deposited ice depends on T_d and is classified into six types: (i) HDA ice at $T_d < 20$ K, (ii) a mixture of HDA and LDA ice at $20 \text{ K} < T_d < 80$ K, (iii) LDA ice at $80 \text{ K} < T_d < 130$ K, (iv) a mixture of LDA ice and I_c at $130 \text{ K} < T_d < 140$ K, (v) I_c at $140 \text{ K} < T_d < 150$ K, and (vi) a mixture of I_c and I_h at $T_d > \sim 150$ K. Furthermore, the processes of the structural transitions from the deposited ice with heating reflect T_d . These results have important implications for the chemical evolution processes in interstellar molecular clouds.



1. INTRODUCTION

In interstellar molecular clouds, the elements such as H, O, C, and N are deposited onto dust grains and form various molecules such as H_2O , CO, CO_2 , CH_3OH , H_2CO , and NH_3 .^{1,2} Most H_2O exists as amorphous ice and covers dust grains as an ice mantle.^{3,4} The included and adsorbed molecules in amorphous ice undergo chemical evolutions to complex organic molecules through various reaction processes.⁵ It is essential to understand the mechanisms of the structural changes of amorphous ice with heating because the surface and interface of amorphous ice act as a reaction field.^{6,7}

Amorphous ice can artificially form using various procedures, such as the pressurization of crystalline ice,⁸ vapor deposition on cold substrates,⁹ ultrarapid quenching of liquid water,¹⁰ and matrix sublimation.¹¹ Vapor deposition is a process similar to the formation of amorphous ice in interstellar molecular clouds. Amorphous ice formed by vapor deposition is mainly classified into two types: high-density amorphous (HDA) and low-density amorphous (LDA) ice.⁹ Using the X-ray diffraction method, Narten et al.⁹ showed that the density of amorphous ice deposited at 10 K is $1.1 \pm 0.1 \text{ g cm}^{-3}$ and higher than that deposited at 77 K ($0.94 \pm 0.03 \text{ g cm}^{-3}$). HDA ice, deposited at lower temperatures, has a higher density owing to its collapsed tetrahedral structure.¹²

HDA ice deposited at low temperatures undergoes phase transitions during heating. Various studies have been performed to investigate the transition process from HDA

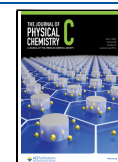
ice after deposition. Based on the measurements of gas evaporation, Laufer et al.¹³ showed that there are at least two types of amorphous ice and that the transition temperature from a low-temperature phase (i.e., HDA ice) to a high-temperature phase is 85 K. From the desorption curve of H_2O for amorphous ice with heating after the deposition at 10 K, Kouchi¹⁴ proposed that amorphous ice is classified into three structures: phase I at $T < 90$ K, phase II at $90 \text{ K} < T < 135$ K, and phase III at $135 \text{ K} < T < 143$ K. Using the electron diffraction method, Jenniskens and Blake¹⁵ investigated the process of the phase transition from HDA ice deposited at 15 K with heating and showed that the HDA ice transforms into LDA ice gradually over the temperature range of 38–68 K. Furthermore, they proposed that the LDA ice transforms into a third phase, which named “restrained” amorphous ice—a precursor of crystalline cubic ice (ice I_c) at 131 K that transforms into ice I_c in the range of 148–188 K. Bolina et al.¹⁶ showed that the deposited ice exists in an amorphous state at temperatures below 135 K, i.e., a glass transition temperature T_g .¹⁷ At temperatures above T_g , amorphous ice undergoes a

Received: March 12, 2024

Revised: April 13, 2024

Accepted: April 22, 2024

Published: May 1, 2024



crystallization. The reported crystallization point of amorphous ice ranges from 130 to 160 K.¹⁸

Ice crystallized from amorphous ice with heating, i.e., ice I_c is a metastable phase.¹⁹ Hansen et al.^{20,21} showed that the ice includes deformation stacking faults. Malkin et al.²² proposed naming the stacking disorder ice, I_{sd} , because its structure consists of cubic and hexagonal sequences. The stacking disorder structure and cubicity depend on the formation and annealing processes.²³ Ice I_{sd} has been mainly observed in relatively thicker samples made by vapor deposition.²⁴ On the other hand, thin samples exist as ice I_c because stacking faults are less likely to be present in thin samples.^{25–27} From the observations using cryogenic transmission electron microscopy (TEM), Kobayashi and Yasuda²⁵ found that deposited ice at 95 K with 20 nm in thickness was ice I_c . From the TEM observation, Kouchi et al.²⁶ showed that ice deposited at 120 K with 45 nm in thickness was also ice I_c . Using reflection high-energy electron diffraction (RHEED), Sato et al.²⁷ showed that ice crystallized at 143 K from amorphous ice with 36 monolayers was a mixture of ice I_c and ice I_h . In addition, pure ice I_c was formed from hydrogen hydrate through an amorphous state and annealing of the ice XVII phase.^{28,29}

Previous results indicate that the transition between amorphous–amorphous phases for vapor-deposited ice occurs at around 38–90 K.^{13–15} However, the mechanism of the phase transition is less conclusive because the transition temperature depends on the formation conditions of the ice samples. In addition, the transition process is affected by inclusions and ultraviolet irradiation. For instance, HDA ice including CO_2 transforms into CO_2 clathrate hydrate with heating.³⁰ The UV-irradiated amorphous ice exhibits a liquid-like viscosity over the temperature range of 50–140 K.³¹

To investigate the effects of the deposition temperature on the transition process of amorphous ice with heating, the infrared (IR) spectra of amorphous ice deposited at temperatures of 6–160 K were measured. Based on the wavenumber of the O–H symmetric stretching mode, the transition temperatures from HDA ice to crystalline hexagonal ice (ice I_h) via LDA ice and ice I_c were analyzed.

2. METHODS

Ice samples were prepared by vapor deposition of water on an oxygen-free copper substrate with a gold coating in a stainless-steel vacuum chamber, which had two KBr windows to transmit the incident and reflected IR beams. The temperature of the substrate was controlled using a Gifford-McMahon (GM) cryocooler (Sumitomo Heavy Industries, RDK-101D). The pressure inside the chamber was maintained at around 3.0×10^{-5} Pa using a turbomolecular pump (Pfeiffer, HiPace 80).

Before deposition, the water was purified by distillation and degassing with two cycles of freezing and thawing. H_2O vapor from the water was introduced into the vacuum chamber through a capillary tube with an inner diameter of 1 mm and deposited on the substrate at a rate of 0.4 nm s^{-1} and a temperature range of 6–160 K. The thickness of the sample immediately after deposition, estimated from the intensity of the O–H stretching mode in the IR spectrum, was maintained at $25 \pm 5 \text{ nm}$. The absorption coefficient of the O–H stretching mode for amorphous ice ($1.7 \times 10^{-16} \text{ cm molecule}^{-1}$) was used to estimate the sample thickness.³² The IR spectra were measured in the wavenumber range of 650–4000 cm^{-1} with a 1 cm^{-1} resolution at 3.2 s intervals during the deposition using a Fourier-transform IR spectrom-

eter (Shimadzu, IRPrestige-21). The angle of the incident infrared beam to the substrate was 20° , with the reflection being detected through the ice sample. After the deposition, the sample was cooled to 6 K and then heated to 176 K at a rate of 5 K min^{-1} . The IR spectra were measured every 3.2 s during the cooling and heating processes. The temperature of the sample was not constant during the measurement of a single spectrum because the temperature-programmed IR was used. However, the influence of the temperature change on a spectrum was negligible because the change in temperature during a measurement was 0.27 K.

3. RESULTS AND DISCUSSION

3.1. Phase Transition with Heating. Figure 1a shows the IR spectra of amorphous ice deposited at 6 K in the

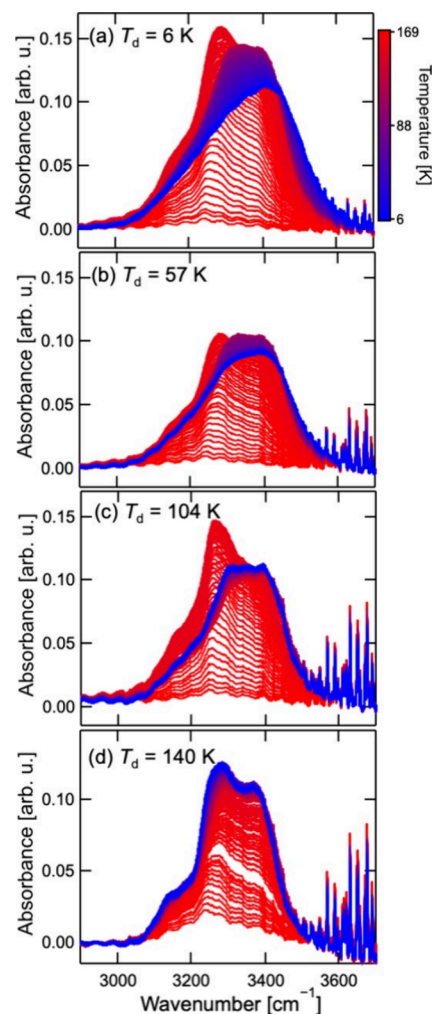


Figure 1. IR spectra of the O–H stretching modes of ice deposited at (a) 6 K, (b) 57 K, (c) 104 K, and (d) 140 K during heating from 6 K.

wavenumber region of the O–H stretching modes during heating from 6 K. The spectral features change with heating, and the peaks disappear at around 170 K owing to the sublimation of water. As several peaks exist in this region, the peak positions were analyzed by fitting the spectrum using three Gaussian functions, as shown in Figure 2. The peaks at 3208, 3294, and 3418 cm^{-1} at 6 K are assigned to the overtone of the O–H bending mode, the O–H asymmetric stretching

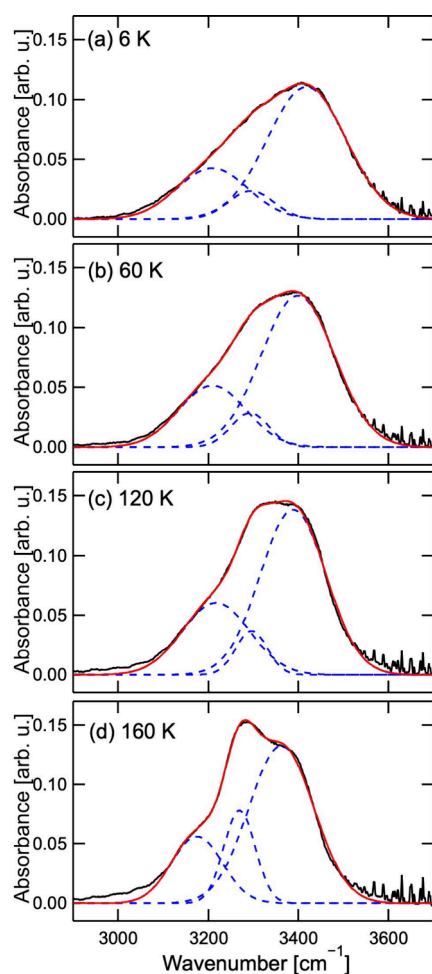


Figure 2. Decomposed spectra of ice at (a) 6 K, (b) 60 K, (c) 120 K, and (d) 167 K during heating from 6 K after the deposition at 6 K. The black solid and blue dashed lines are the experimental data and fitting curves, respectively. The red lines are the sum of the fitting curves.

mode, and the O–H symmetric stretching mode of H₂O, respectively.³³

Figure 3a shows the temperature dependence of the wavenumber of the O–H symmetric stretching mode of the amorphous ice deposited at 6 K with heating. As shown in Figure 4, the changing rate of the wavenumber with temperature changes at 23, 95, 152, and 167 K. The wavenumbers are approximately constant at temperatures below 23 K. In this range, vapor-deposited ice exists as HDA ice.^{13–15} For liquid water and crystalline ice, the wavenumber of the O–H stretching mode increases with heating owing to thermal expansion because the wavenumber of the O–H stretching mode increases owing to a decrease in the strength of hydrogen bonds. In the case of HDA ice, no increase was observed in the wavenumber with heating because the relaxation of the collapsed structure proceeds preferentially.

The wavenumber of the O–H symmetric stretching mode gradually decreases from 23 to 95 K. This indicates that the transition from HDA to LDA ice begins at around 23 K. The O–H symmetric stretching mode of LDA ice is lower than that of HDA ice because the hydrogen bond in LDA ice is stronger.³⁴ HDA ice transforms into LDA ice owing to the relaxation of the collapsed structure.¹⁵ The beginning temperature of the transition from HDA to LDA ice (i.e., 23 K) is

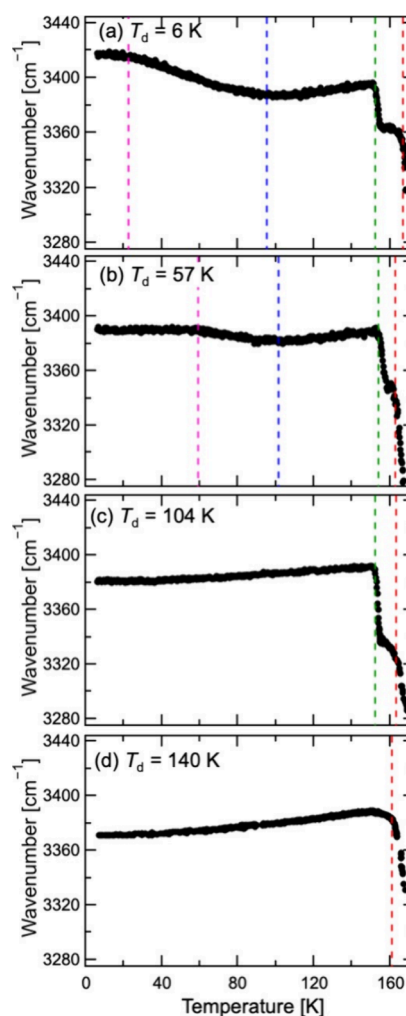


Figure 3. Temperature dependences of peak position of the O–H symmetric stretching mode of ice with heating from 6 K after the cooling from the deposition temperature T_d of (a) 6 K, (b) 57 K, (c) 104 K, and (d) 140 K. The pink and blue dashed lines show the temperatures at the beginning and end of the transition from HDA ice to LDA ice, respectively. The green and red dashed lines are the transition temperatures from LDA ice to ice I_c and from ice I_c to ice I_h , respectively.

close to the temperature of the pore collapse in the porous amorphous solid water (pASW).³⁵ This suggests that the transition from HDA to LDA ice is a cause of the pore collapse in pASW. The relative amount of LDA ice increases with heating, and the transition concludes at around 95 K. At temperatures above 95 K, the wavenumber gradually increases with the thermal expansion of the LDA ice.

Drastic decreases in the wavenumbers of the O–H stretching mode are observed at around 152 and 167 K. Figure 5a shows that the spectral features change significantly in the temperature range of 152–155 K. The decrease in wavenumber at around 152 K is attributed to the crystallization from LDA ice, considering the spectral feature at 155 K is similar to that of crystalline ice I.³⁶ Although ice I is I_c , I_h , or a mixture of I_c and I_h ,^{25–27} the ice samples of the present study were assigned to ice I_c because the thicknesses of the samples were thin enough (25 ± 5 nm). As shown in Figures 4d and 5b, no significant changes in the spectral feature and wavenumber are observed in the range of 156–164 K. This

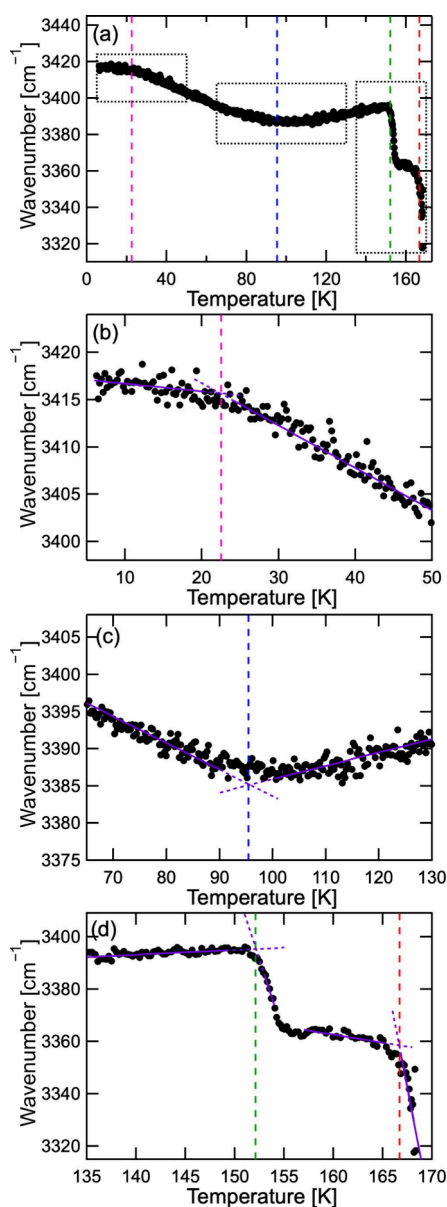


Figure 4. Enlarged figures of temperature dependence of peak position of the O–H symmetric stretching mode of ice with $T_d = 6$ K (a). (b,c) Enlarged figures around the beginning and end of the transition from HDA ice to LDA ice, respectively. (d) Enlarged figure in the range of the crystallization. The purple dotted lines are the fitted lines to determine the transition temperatures.

indicates that the transition from LDA ice to ice I_c approximately completed in the temperature range of 152–155 K, which corresponds to about 36 s. At temperatures above 167 K, the O–H stretching band shifts to lower wavenumbers, as shown in Figures 4d and 5c. The significant decrease in wavenumber at around 167 K is attributed to the transition from ice I_c to ice I_h via I_{sd} .³⁷ This temperature is consistent with the reported transition temperature from ice I_{sd} to ice I_h (160–240 K).³⁸ The hydrogen bonds of ice I_h is slightly stronger than that of I_{sd} . The average O–O distance between hydrogen-bonded water molecules in ice I_h (0.2752 nm at 123 K³⁹) is slightly smaller than that in I_{sd} (0.2755 nm at >120 K³⁴). In the case of the transition from pure I_c to I_h , the O–H stretching band shifts to a higher wavenumber.⁴⁰ This

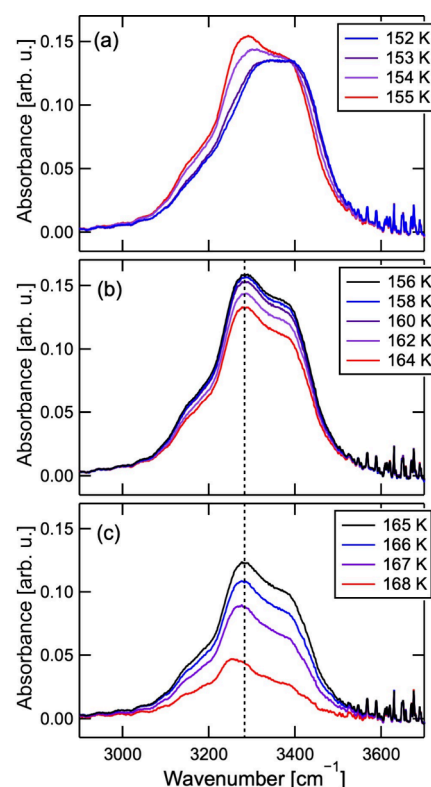


Figure 5. Variations of IR spectra in the temperature range of (a) 152–155 K, (b) 156–164 K, and (c) 165–168 K during heating from 6 K after the deposition at 6 K. The dotted lines are the guides to show the trends of the band shift.

suggests that the stacking disordered structure in I_{sd} causes a decrease in the strength of the hydrogen bonds.

3.2. Effects of Deposition Temperature on the Ice Structure. The structure of ice after cooling from the deposition temperature, T_d , reflects the structure at the moment of its deposition. The blue lines in Figure 1b–d show the IR spectra of ice deposited at 57, 104, and 140 K after cooling to 6 K from their T_d . The spectral features at 6 K depend on T_d . The spectra for ice with $T_d = 57$ and 104 K are broad in comparison with that of $T_d = 6$ K, whereas the spectrum for ice with $T_d = 140$ K is sharp. The spectral features of ice with $T_d = 140$ K are similar to those of ice I_c .³⁶

Figure 6 shows the wavenumber of the O–H symmetric stretching mode at 6 K after cooling from T_d as a function of T_d . Based on the decreasing rate of the wavenumber with T_d , the deposited ice is classified into six structures: (i) HDA at $T_d < 20$ K, (ii) a mixture of HDA and LDA at 20 K $< T_d < 80$ K, (iii) LDA at 80 K $< T_d < 130$ K, (iv) a mixture of LDA and I_c at 130 K $< T_d < 140$ K, (v) I_c at 140 K $< T_d < 150$ K, and (vi) a mixture of I_c and I_h at $T_d > \sim 150$ K. The wavenumbers in the ranges of $T_d < 20$ K, 80 K $< T_d < 130$ K, and 140 K $< T_d < 150$ K are approximately constant, respectively. Therefore, the structures in these temperature ranges are assigned to the pure states of HDA, LDA, and I_c , respectively, instead of the mixed states. The decrease in the wavenumber observed at 20 K $< T_d < 80$ K indicates that HDA and LDA ices coexist in this temperature range, and the relative amount of LDA increases as the deposition temperature increases.

The drastic decrease in the wavenumber observed at 130 K $< T_d < 140$ K indicates that the deposited ice includes ice I_c and that the relative amount of ice I_c increases as the

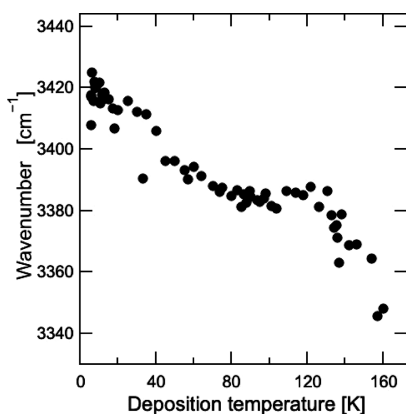


Figure 6. Peak position of the O–H symmetric stretching mode of ice after cooling to 6 K as a function of the deposition temperature T_d .

deposition temperature increases. The beginning temperature (130 K) is lower than the beginning temperature for the formation of I_c with heating (i.e., 152 K for the ice with $T_d = 6$ K, as described in Section 3.1.). The result suggests that the activation energy for the transition from water vapor to ice I_c is lower than that of LDA ice. In the case of crystallization from amorphous ice, the nucleation of ice crystals in amorphous ice occurs randomly, with the growth rate dependent on temperature.³⁶ Using the reported crystallization time, i.e., the time required for the 100% conversion from amorphous ice to crystal, in the temperature range of 152–172 K,⁴¹ the crystallization time from LDA at 130 K is estimated to be 4.7×10^6 s. The crystallization time decreases with heating, reaching 5.0×10^3 s at 152 K. Thus, the formation of ice I_c was observed at 152 K in the case of heating of amorphous ice with $T_d = 6$ K.

The drastic decrease in wavenumber observed at around 150 K in Figure 6 indicates that a mixture of ice I_c and I_h is deposited at temperatures above 150 K. This temperature is also lower than the transition temperature from ice I_c to ice I_h (167 K for ice with $T_d = 6$ K) owing to the transition from water vapor.

3.3. Effects of Deposition Temperature on the Phase Transition Process. As shown in Figure 1b–d, the changing process in the spectral features with heating depends on the deposition temperature. Hence, the spectral changes with heating were analyzed to investigate the effects of the deposition temperature on the transition processes. Figure 3b–d shows the temperature dependence of the wavenumber of the O–H symmetric stretching mode of ice deposited at 57, 104, and 140 K with heating after cooling to 6 K from T_d . In the case of $T_d = 57$, four transitions are observed at 59, 102, 154, and 163 K, although the transition temperatures differ from those for $T_d = 6$ K. In contrast, only one or two transition points are observed in the cases of $T_d = 104$ and 140 K.

Figure 7 shows the transition points as functions of T_d . The two lower transition points (pink and blue circles) are observed at deposition temperatures below 95 K. The first- and second-lowest points are at the beginning and end of the transition from HDA ice to LDA ice, respectively. These results indicate that the deposited ice includes HDA at temperatures below 95 K. In the range of $T_d = 95$ –133 K, the deposited ice exists as pure LDA ice. As indicated by the dotted line, the beginning points denoted by pink circles are approximately consistent with the deposition points at the temperatures. This suggests that the structure and composition

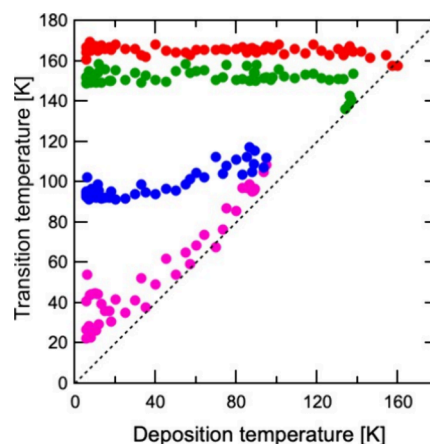


Figure 7. Dependences of transition temperatures on deposition temperature T_d from the IR spectra with heating. The pink and blue circles show the beginning and end of the transition from HDA ice to LDA ice, respectively. The green and red circles are the transition temperatures from LDA ice to ice I_c and from ice I_c to ice I_h , respectively. The dotted line shows a point at which the transition temperature is equal to T_d .

of the mixture of deposited ice are stable during cooling and heating at temperatures below T_d .

The green and red circles represent the beginning points of crystallization from LDA ice to ice I_c and the phase transition from I_c to I_h , respectively. These temperatures are independent of T_d . This indicates that the deposition conditions do not affect the structure of the LDA ice after the transition from HDA ice with heating. As described in Section 3.2., the deposited ice exists as I_c , ice I_h , or their mixture at $T_d > \sim 140$ K. Thus, the transition point denoted by the green circle disappears, and only a transition to ice I_h occurs. The dispersion observed at around 140 K implies that the mixtures are inhomogeneous.

3.4. Effects of the Surface Structure on the Phase Transition Process. As shown by the pink circles in Figure 7, the beginning point of the transition from HDA ice to LDA ice disperses at temperatures below 20 K. For instance, the maximum and minimum transition points for ice deposition at 6 K were 23 and 54 K, respectively. The red and blue symbols in Figure 8 show the temperature dependence of the wavenumber of the O–H symmetric stretching mode of amorphous ice deposited at 6 K with the maximum and minimum transition points. As shown in Figure 8, ice with a

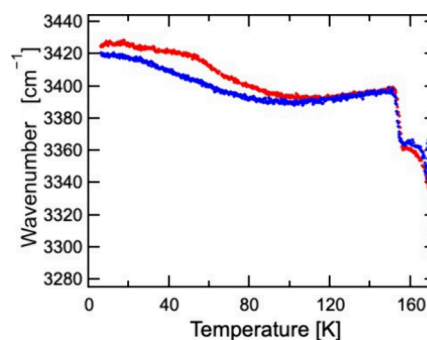


Figure 8. Temperature dependence of wavenumber of the O–H symmetric stretching mode of two samples with $T_d = 6$ K with heating.

higher wavenumber in the O–H symmetric stretching mode at 6 K has a higher transition point from HDA ice to LDA ice. The difference in the wavenumbers is attributed to the difference in the specific surface area of the deposited HDA ice.

The density of HDA ice is higher than that of LDA ice because of the existence of interstitial molecules between the first and second neighbors.⁴² The transition from HDA ice to LDA ice occurs due to a relaxation of the distorted structure. However, in the case of HDA ice with a large specific surface area, surface relaxation may alleviate structural distortion. As shown by the red symbols in Figure 8, for ice with a higher wavenumber of the O–H symmetric stretching mode at 6 K, the higher wavenumber was maintained at temperatures below the beginning point of the transition to LDA (i.e., 54 K). This indicates that the purity of HDA ice in this sample is higher than that of another sample denoted by the blue line because the wavenumber of the O–H symmetric stretching mode of HDA ice is higher than that of LDA ice.³⁴ The large surface area caused by pores and cracks might affect the formation of pure HDA ice to defuse tension from the distorted structure of HDA ice.⁴³

4. CONCLUSIONS

The IR spectra of the deposited ice at temperatures of 6–160 K were measured to investigate the effects of deposition temperature on the phase transition process of ice with heating. The results show that the deposited ice can be classified into six types: (i) HDA at $T_d < 20$ K; (ii) a mixture of HDA and LDA at $20 \text{ K} < T_d < 80$ K; (iii) LDA at $80 \text{ K} < T_d < 130$ K; (iv) a mixture of LDA and ice I_c at $130 \text{ K} < T_d < 140$ K; (v) ice I_c at $140 \text{ K} < T_d < 150$ K; and (vi) a mixture of ice I_c and ice I_h at $T_d > 150$ K. At temperatures above 20 K, the structure and composition of the mixture of deposited ice remains stable during cooling and heating at temperatures below T_d . The transition from HDA to LDA ice occurs gradually with heating at temperatures above T_d . The structure of LDA ice is independent of the deposition conditions and thermal history after deposition. Furthermore, the transition temperature from HDA to LDA ice reflects the surface structure of the deposited HDA ice at $T_d < 20$ K. The structure of the deposited ice and the transition temperatures might depend on the deposition rate and heating rate after the deposition because the deposition rate and heating rate have effects on the structural changes.^{3,44,45} The temperature dependence of the structure during deposition and the phase transition temperature during heating determined in this study are those at the deposition rate = 0.4 nm s^{-1} and the heating rate = 5 K min^{-1} , respectively. However, the present results suggest that the ice structure can be a measure of the thermal history of ice in interstellar molecular clouds.

AUTHOR INFORMATION

Corresponding Author

Tomoko Ikeda-Fukazawa – Department of Applied Chemistry, Meiji University, Kawasaki 214-8571, Japan;
orcid.org/0000-0002-5265-4706; Email: fukazawa@meiji.ac.jp

Authors

Kentaro Kina – Department of Applied Chemistry, Meiji University, Kawasaki 214-8571, Japan

Yui Ono – Department of Applied Chemistry, Meiji University, Kawasaki 214-8571, Japan

Daiki Yoshida – Department of Applied Chemistry, Meiji University, Kawasaki 214-8571, Japan

Complete contact information is available at:
<https://pubs.acs.org/10.1021/acs.jpcc.4c01617>

Author Contributions

T.I.-F. designed the research, and K.K., Y.O., and D.Y. conducted the experiments and analysis. All authors discussed the data and wrote the paper.

Notes

The authors declare no competing financial interest.

ACKNOWLEDGMENTS

This study was supported by MEXT KAKENHI Grant Numbers 21H01151 and 23H03995.

REFERENCES

- (1) Ehrenfreund, P.; Charnley, S. B. Organic molecules in the interstellar medium, comets, and meteorites: a voyage from dark clouds to the early earth. *Astron. Astrophys.* **2000**, *38*, 427–483.
- (2) Pontoppidan, K. M.; Dartois, E.; van Dishoeck, E. F.; Thi, W. F. Detection of abundant solid methanol toward young low mass stars. *Astron. Astrophys.* **2003**, *404*, L17–L20.
- (3) Kouchi, A.; Yamamoto, T.; Kozasa, T.; Kuroda, T.; Greenberg, J. M. Conditions for condensation and preservation of amorphous ice and crystallinity of astrophysical ices. *Astron. Astrophys.* **1994**, *290*, 1009–1018.
- (4) Keane, J.; Tielens, A. G. G. M.; Boogert, A. C. A.; Schutte, W. A.; Whittet, D. C. B. Ice absorption features in the 5–8 μm region toward embedded protostars. *Astron. Astrophys.* **2001**, *376*, 254–270.
- (5) Watanabe, N.; Kouchi, A. Efficient formation of formaldehyde and methanol by the addition of hydrogen atoms to CO in H₂O–CO ice at 10 K. *Astrophys. J.* **2002**, *571*, L173–L176.
- (6) Kumagai, Y.; Ikeda-Fukazawa, T. Structures of surface and interface of amorphous ice. *Chem. Phys. Lett.* **2017**, *678*, 153–158.
- (7) Aoki, M.; Hara, N.; Ikeda-Fukazawa, T. Surface diffusion of proton in amorphous ice. *Surf. Sci.* **2019**, *684*, 58–61.
- (8) Mishima, O.; Calvert, L. D.; Whalley, E. ‘Melting’ I at 77 K and 10 kbar: a new method of making amorphous solids. *Nature* **1984**, *310*, 393–395.
- (9) Narten, A. H.; Venkatesh, C. G.; Rice, S. A. Diffraction pattern and structure of amorphous solid water at 10 and 77 K. *J. Chem. Phys.* **1976**, *64*, 1106–1121.
- (10) Brüggeller, P.; Mayer, E. Complete vitrification in pure liquid water and dilute aqueous solutions. *Nature* **1980**, *288*, 569–571.
- (11) Kouchi, A.; Hama, T.; Kimura, Y.; Hidaka, H.; Escribano, R.; Watanabe, N. Matrix sublimation method for the formation of high-density amorphous ice. *Chem. Phys. Lett.* **2016**, *658*, 287–292.
- (12) Jenniskens, P.; Blake, D. F.; Wilson, M. A.; Pohorille, A. High-density amorphous ice, the frost on interstellar grains. *Astrophys. J.* **1995**, *455*, 389–401.
- (13) Laufer, D.; Kochavi, E.; Bar-Nun, A. Structure and dynamics of amorphous water ice. *Phys. Rev. B* **1987**, *36*, 9219–9228.
- (14) Kouchi, A. Evaporation of H₂O–CO ice and its astrophysical implications. *J. Cryst. Growth* **1990**, *99*, 1220–1226.
- (15) Jenniskens, P.; Blake, D. F. Structural transitions in amorphous water ice and astrophysical implications. *Science* **1994**, *265*, 753–756.
- (16) Bolina, A. S.; Wolff, A. J.; Brown, W. A. Reflection absorption infrared spectroscopy and temperature-programmed desorption studies of the adsorption and desorption of amorphous and crystalline water on a graphite surface. *J. Phys. Chem. B* **2005**, *109*, 16836–16845.
- (17) Hallbrucker, A.; Mayer, E.; Johari, G. P. Glass-liquid transition and the enthalpy of devitrification of annealed vapor-deposited amorphous solid water: a comparison with hyperquenched glassy water. *J. Phys. Chem.* **1989**, *93*, 4986–4990.

- (18) Lofgren, P.; Ahlstrom, P.; Lausma, J.; Kasemo, B.; Chakarov, D. Crystallization kinetics of thin amorphous water films on surfaces. *Langmuir* **2003**, *19*, 265–274.
- (19) Murray, B. J.; Bertram, A. K. Formation and stability of cubic ice in water droplets. *Phys. Chem. Chem. Phys.* **2006**, *8*, 186–192.
- (20) Hansen, T. C.; Koza, M. M.; Kuhs, W. F. Formation and annealing of cubic ice: I. modelling of stacking faults. *J. Phys.: Condens. Matter* **2008**, *20*, No. 285104.
- (21) Hansen, T. C.; Koza, M. M.; Lindner, P.; Kuhs, W. F. Formation and annealing of cubic ice: II. kinetic study. *J. Phys.: Condens. Matter* **2008**, *20*, No. 285105.
- (22) Malkin, T. L.; Murray, B. J.; Brukhno, A. V.; Anwar, J.; Salzmänn, C. G. Structure of ice crystallized from supercooled water. *Proc. Natl. Acad. Sci. U.S.A.* **2012**, *109*, 1041–1045.
- (23) Ladd-Parada, M.; Amann-Winkel, K.; Kim, K. H.; Späh, A.; Perakis, F.; Pathak, H.; Yang, C.; Mariedahl, D.; Eklund, T.; Lane, T. J.; et al. Following the crystallization of amorphous ice after ultrafast laser heating. *J. Phys. Chem. B* **2022**, *126*, 2299–2307.
- (24) Malkin, T. L.; Murray, B. J.; Salzmänn, C. G.; Molinero, V.; Pickering, S. J.; Whale, T. F. Stacking disorder in ice I. *Phys. Chem. Chem. Phys.* **2015**, *17*, 60–76.
- (25) Kobayashi, K.; Yasuda, H. Phase transition of ice Ic to ice XI under electron beam irradiation. *Chem. Phys. Lett.* **2012**, *547*, 9–12.
- (26) Kouchi, A.; Yamazaki, T.; Katsuno, H.; Nada, H.; Hama, T.; Kimura, Y. Observation of hydrogen-ordered cubic ice thin films on the surface of ice Ic nanocrystals upon coarsening. *Chem. Phys.* **2023**, *527*, No. 111966.
- (27) Sato, R.; Taniguchi, S.; Numadate, N.; Hama, T. Structure of crystalline water ice formed through neon matrix sublimation under cryogenic and vacuum conditions. *J. Chem. Phys.* **2023**, *158*, 211101.
- (28) Komatsu, K.; Machida, S.; Noritake, F.; Hattori, T.; Sano-Furukawa, A.; Yamane, R.; Yamashita, K.; Kagi, H. Ice Ic without stacking disorder by evacuating hydrogen from hydrogen hydrate. *Nat. Commun.* **2020**, *11*, 464.
- (29) Rosso, L. D.; Celli, M.; Grazzi, F.; Catti, M.; Hansen, T. C.; Fortes, A. D.; Ulivi, L. Cubic ice Ic without stacking defects obtained from ice XVII. *Nat. Mater.* **2020**, *19*, 663–668.
- (30) Netsu, R.; Ikeda-Fukazawa, T. Structures of surface and interface of amorphous ice. *Chem. Phys. Lett.* **2017**, *678*, 153–158.
- (31) Tachibana, S.; Kouchi, A.; Hama, T.; Oba, Y.; Piani, L.; Sugawara, I.; Endo, Y.; Hidaka, H.; Kimura, T.; Murata, K.; et al. Liquid-like behavior of UV-irradiated interstellar ice analog at low temperatures. *Sci. Adv.* **2017**, *3*, No. eaao2538.
- (32) Hudgins, D. M.; Sandford, S. A.; Allamandola, L. J.; Tielens, A. G. M. Mid- and far infrared spectroscopy of ices -optical constants and integrated absorbance. *Astrophys. J.* **1993**, *86*, 713–870.
- (33) Haas, C.; Hornig, D. F. Inter- and intramolecular potentials and the spectrum of ice. *J. Chem. Phys.* **1960**, *32*, 1763–1769.
- (34) Karina, A.; Eklund, T.; Tonauer, C. M.; Li, H.; Loerting, T.; Amann-Winkel, K. Infrared spectroscopy on equilibrated high-density amorphous ice. *J. Phys. Chem. Lett.* **2022**, *13*, 7965–7971.
- (35) Kouchi, A.; Furuya, K.; Hama, T.; Chigai, T.; Kozasa, T.; Watanabe, N. Direct measurements of activation energies for surface diffusion of CO and CO₂ on amorphous solid water using in situ transmission electron microscopy. *Astrophys. J. Lett.* **2020**, *891*, L22.
- (36) Hama, T.; Ishizuka, S.; Yamazaki, T.; Kimura, Y.; Kouchi, A.; Watanabe, N.; Sugimoto, T.; Pirronello, V. Fast crystalline ice formation at extremely low temperature through water/neon matrix sublimation. *Phys. Chem. Chem. Phys.* **2017**, *19*, 17677–17684.
- (37) Carr, T. H. G.; Shephard, J. J.; Salzmänn, C. G. Spectroscopic signature of stacking disorder in ice I. *J. Phys. Chem. Lett.* **2014**, *5*, 2469–2473.
- (38) Tonauer, C. M.; Yamashita, K.; del Rosso, L.; Celli, M.; Loerting, T. Enthalpy change from pure cubic ice I_c to hexagonal ice I_h. *J. Phys. Chem. Lett.* **2023**, *14*, 5055–5060.
- (39) Kuhs, W. F.; Lehmann, M. S. *The structure of ice Ih*. *Water Science Review* 2; Cambridge Univ. Press, 1986.
- (40) Celli, M.; Ulivi, L.; Rosso, L. Raman investigation of the ice Ic–ice Ih transformation. *J. Phys. Chem. C* **2020**, *124*, 17135–17140.
- (41) Kondo, T.; Kato, H. S.; Bonn, M.; Kawai, M. Morphological change during crystallization of thin amorphous solid water films on Ru(0001). *J. Chem. Phys.* **2007**, *126*, 181103.
- (42) Amann-Winkel, K.; Bellissent-Funel, M. C.; Bove, L. E.; Loerting, T.; Nilsson, A.; Paciaroni, A.; Schlesinger, D.; Skinner, L. X-ray and neutron scattering of water. *Chem. Rev.* **2016**, *116*, 7570–7589.
- (43) Stevenson, K. P.; Kimmel, G. A.; Dohnalek, Z.; Smith, R. S.; Kay, B. D. Controlling the morphology of amorphous solid water. *Science* **1999**, *283*, 1505–1507.
- (44) Krikorian, E.; Sneed, R. J. Epitaxial deposition of germanium by both sputtering and evaporation. *J. Appl. Phys.* **1966**, *37*, 3665–3673.
- (45) Yamazaki, T.; Kouchi, A.; Murata, K.; Katsuno, H.; Nada, H.; Hama, T.; Kimura, Y. In situ cryogenic transmission electron microscopy observation on the formation of hydrogen-ordered hexagonal ices and its astrophysical implications. *Mon. Not. R. Astron. Soc.* **2023**, *527*, 2858–2868.